On Tungstates of Divalent Cations (II) – Polymorphy of Pb_2WO_5

Stephan G. Jantz,[a] Florian Pielnhofer,[b] Marwin Dialer,[a] and Henning A. Höppe*[a]

Dedicated to Professor Thomas Schleid on the Occasion of his 60th Birthday

Abstract. The phase transition from the low temperature form $Pb_2[WO_5]$ to its high temperature form $Pb_2O[WO_4]$ was monitored by means of temperature dependent powder XRD. Single-crystals of $Pb_2[WO_5]$, suitable for a structure determination by single-crystal X-ray diffraction, were obtained by quenching a sample from 500 °C to room temperature. The low-temperature phase $Pb_2[WO_5]$ comprises the structural motive of infinite zigzag chains built by cornersharing WO_6 octahedra, known from the tungstates $M_2[WO_5]$ (M = Sr, Ba), but crystallizes in a new structure type [$C2/c$, a = 14.0996(4) Å, b = 5.8579(2) Å, c = 12.6877(4) Å, β = 114.3569(13)°, Z = 8, R_{int} = 0.042, R_1 = 0.040, wR_2 = 0.068]. The crystal structure of the high-temperature phase $Pb_2O[WO_4]$ [$C2/m$, a = 14.2126(4) Å, b = 5.80150(10) Å, c = 7.3477(2) Å, β = 113.9402(7)°, Z = 4, R_1 = 0.035, wR_2 = 0.055] is revised, based on single-crystal XRD data. Furthermore spectroscopic data (IR, Raman and UV/Vis spectra) are presented.

Introduction

As mentioned in our first contribution on tungstates of divalent cations[1] we are interested in new phosphors, which might be sensitized by the allowed charge-transfer transition typical for transition metals in high oxidation states. Moreover, we are interested in condensed anionic network structures, which we classify as silicate-analogous if comprising tetrahedral basic building units as found in borosulfates[2,3] or the tungstate phosphates $Na_2RE[PO_4][WO_4]$ (RE = Y, Dy – Lu) and $Na_2Y[PO_4][WO_4]$:Ln^{3+} (Ln = Eu, Tb).[4]

During our investigations on $AE_2[WO_5]$ (AE = Sr, Ba) compounds,[1] we came across the – on first glance – homologous lead compound comprising an analogous chemical formula but a different anionic topology (ICSD entry no. 61399[5]). Instead of infinite zigzag chains built by corner-sharing WO_6 octahedra, HT-$Pb_2O[WO_4]$[6] (HT = high-temperature) comprises non-condensed WO_4 tetrahedra and chains of edge-sharing OPb_4 tetrahedra. *DeVries* and *Fleischer*[7] describe a "considerable structure change" in the system PbO·$PbWO_4$ on cooling from high temperatures to room temperature. Furthermore *Fujita* and *Muramatsu*[8] investigated this phase transformation in more detail and postulated HT-$Pb_2O[WO_4]$ to be isotypic with Pb_2MoO_5.[9] The crystal structure of HT-$Pb_2O[WO_4]$ was solved in addition by *Bosselet* et al. via powder X-ray diffraction.[6]

* Prof. Dr. H. A. Höppe
E-Mail: henning@ak-hoeppe.de
[a] Lehrstuhl für Festkörperchemie
Universität Augsburg
Universitätsstraße 1
86159 Augsburg, Germany
[b] Abteilung Nanochemie
Max-Planck-Institut für Festkörperforschung
Heisenbergstr. 1
70569 Stuttgart, Germany
Supporting information for this article is available on the WWW under **http://dx.doi.org/10.1002/zaac.201700335** or from the author.

Lead compounds are of interest also for their optical properties as Pb^{2+} ions are subject to parity-allowed $s^2 \rightarrow s^1p^1$ transitions. In this contribution we present the crystal structures of both, the high- and low-temperature forms of Pb_2WO_5, solved from single-crystal X-ray diffraction data. We shed further light on the phase transition and present relevant spectroscopic data and an interpretation thereof.

Results and Discussion

Crystal Structure of LT-Pb_2WO_5 – $Pb_2[WO_5]$

The low temperature form of LT-Pb_2WO_5, i.e. $Pb_2[WO_5]$ crystallizes in a new structure type in the monoclinic space group $C2/c$ (no. 15) with eight formula units per unit cell; it is illustrated in Figure 1. All atoms occupy the general *Wyckoff* site 8*f*.

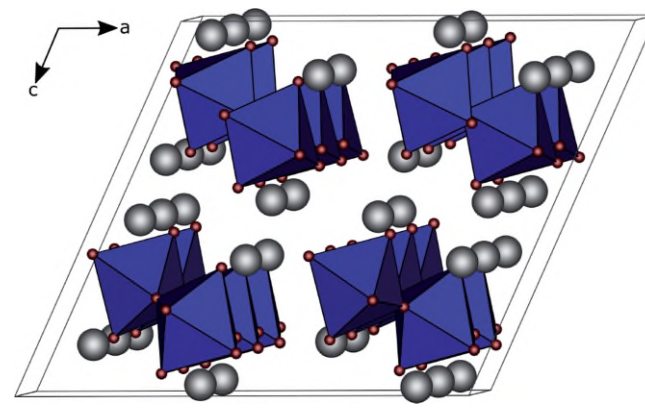

Figure 1. The crystal structure of $Pb_2[WO_5]$ viewed along [010]; lead grey, oxygen red, WO_6 octahedra blue.

Likewise in $Sr_2[WO_5]$ (**1**) and $Ba_2[WO_5]$ (**2**),[1] the crystal structure is built up by corner-sharing distorted WO_6 octahedra, forming infinite zigzag chains along the [010] direction,

which are flanked by Pb^{2+} cations (Figure 1). In the well-known structures of **1** and **2** the same zigzag chains are found. But in contrast to those the Pb and W atoms in $Pb_2[WO_5]$ form distorted closest packed layers perpendicular to the *b* axis (length approx. 5.85 Å) and an AB layer sequence, thus forming a distorted *hcp*. The analogous *M*–W atom layers in **1** and **2** also follow an AB layer sequence, but the layers perpendicular to the *c* axis in **1** and the *b* axis in **2** (length approx. 5.54 Å and 5.71 Å, respectively) only comprise fragments of hexagonal layers, in which W1 and *M*2 are coordinated fivefold within the layer, whereas the *M*1 atoms are coordinated sixfold as expected for such a layer.

The WO_6 chains are tilted stronger in $Pb_2[WO_5]$ (Figure 2) compared with $Sr_2[WO_5]$ (space group $Pna2_1$) as well as $Ba_2[WO_5]$ (space group *Pnma*), which is presumably an effect of the heavy out-of-center distortion of the WO_6 octahedron (Figure 3). This in turn is observed frequently in octahedrally coordinated d^0 transition metal ions.[10] The average W–O distance of 1.96 Å matches very well with the sum of the effective ionic radii of 2.0 Å,[11] whereupon this average calculates from distances in the range 1.77–2.31 Å (Table 1). Although 2.31 Å is a rather large value for a W–O bond distance, O1 contributes twice to the coordination of W1, according to our MAPLE calculation[12–14] (Table S1, Supporting Information). The O–W–O angles of the fundamental building unit (FBU) WO_6 also show a wide range of 76.7–104.2° for adjacent neighbors.

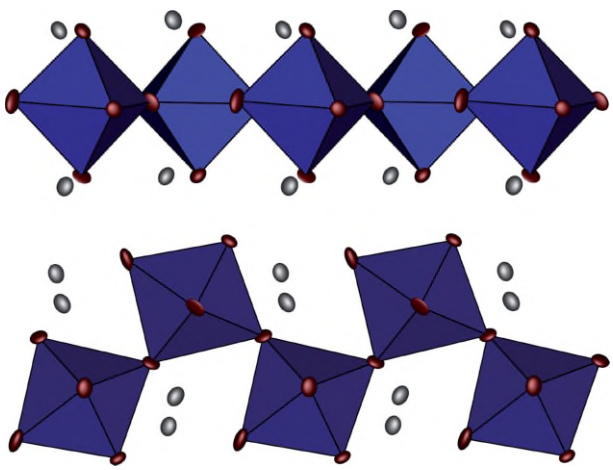

Figure 2. Side (top) and top (bottom) view of the tilted WO_6 chains in $Pb_2[WO_5]$; lead grey, oxygen red, WO_6 octahedra blue; all atoms are drawn with their displacement ellipsoids at a 95% probability level.

The Pb^{2+} cations occupy two distinct crystallographic sites, which are coordinated eight- and sixfold by oxygen atoms in the case of Pb1 and Pb2, respectively. The coordination polyhedra can be described as distorted snub disphenoid (Johnson polyhedron J_{84}) for Pb1 and as distorted triangular prism for Pb2 (Figure S1, Supporting Information). Only oxygen atoms up to a distance of 3.07 Å were considered, due to the result of our MAPLE calculation shown in Table S2 (Supporting Information). The Pb–O distances are in the range 2.37–3.07 Å

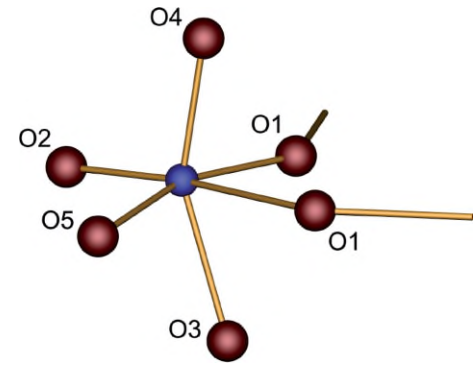

Figure 3. Distorted WO_6 octahedron in $Pb_2[WO_5]$; lead grey, tungsten blue, oxygen red; the O1 atoms are bridging to further WO_6 octahedra.

Table 1. Relevant interatomic distances /Å and angles /° in $Pb_2[WO_5]$ (esds in parentheses).

Pb1–O	2.373(12)–3.069(13)
Pb2–O	2.400(11)–2.894(12)
W–O1	1.913(11)–2.309(12)
W–O2	1.771(13)
W–O3	2.031(11)
W–O4	1.840(12)
W–O5	1.894(11)
O_{term}–W–O_{term} (adj.)[a]	85.5(5)–104.2(6)
O_{term}–W–O_{term} (opp.)[a]	153.6(5)
O_{term}m–W–O_{brid}[a]	76.7(5)–97.3(5)
O_{brid}–W–O_{brid}[a]	90.4(2)
W–O_{brid}–W[a]	142.9(6)

a) O_{term} = terminal oxygen atom, O_{brid} = bridging oxygen atom, adj. = adjacent neighbor, opp. = opposite neighbor.

fwith average values of 2.54 Å and 2.43 Å for Pb1 and Pb2, respectively (Table 1).

Crystal Structure of HT-Pb_2WO_5 – $Pb_2O[WO_4]$

When heated, the low-temperature polymorph transforms into the high temperature modification HT-Pb_2WO_5, i.e. $Pb_2O[WO_4]$,[15] in the monoclinic space group *C*2/*m* (no. 12) with four formula units per unit cell. Its crystal structure was already determined by *Bosselet* et al. in 1985 based on powder diffraction data, and here we present the structure model based on single-crystal diffraction data with a special focus on the anisotropic displacement parameters, which gave indication for twinning and disorder in $Sr_2[WO_5]$.[1] The cations Pb^{2+} and W^{6+} sit on Wyckoff position 4*i* and the anions on 4*g*, 4*i* and 8*j* (cf. Table S6, Supporting Information). Our structure solution obtained from single-crystal X-ray diffraction coincides with the previously reported data, extending these by anisotropic displacement parameters, which are interestingly inconspicuous (Figure 5, Table 4, and Tables S6 and S7, Supporting Information). For a comprehensible description the structure can be subdivided into an anionic and cationic partial structure, where the anionic partial structure comprises non-condensed WO_4 tetrahedra and single O^{2-} anions (O1) coordinated by four Pb^{2+} cations, forming chains of edge-sharing OPb_4 tetrahedra along the [010] direction (Figure 4).

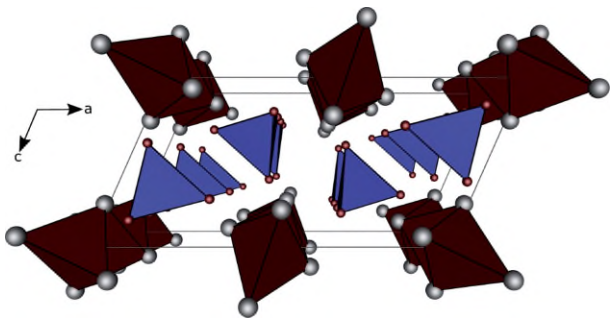

Figure 4. Crystal structure of $Pb_2O[WO_4]$ viewed along [010]; lead grey, oxygen red, WO_4 tetrahedra blue, OPb_4 tetrahedra dark red.

The average W–O distance of 1.77 Å corresponds to the sum of the effective ionic radii[11] of 1.80 Å with a low spread of 1.77–1.79 Å. The O–W–O angles range from 106.8–111.4° resulting in a mean value of 109.46° (Table 2). The deviation of the WO_4 moiety from ideal tetrahedral symmetry is rather low with a value of –0.24 % and was calculated employing the method of *Balić-Žunić* and *Makovicky* based on all ligands enclosing spheres on experimental data.[16,17] While all Pb–O1 distances in the OPb_4 tetrahedron are nearly equal [2.304(3) Å], the Pb–O1–Pb angles vary in a range of 100.6–117.9°, resulting in a larger deviation from tetrahedral symmetry of –1.99 %.

Table 2. Relevant ranges of interatomic distances /Å and angles /° in $Pb_2O[WO_4]$ (esds in parentheses).

Pb1–O	2.305(2)–2.630(4)
Pb2–O	2.304(2)–2.880(5)
O1–Pb	2.304(2)–2.305(2)
W–O	1.766(3)–1.790(5)
Pb–O1–Pb	100.63(14)–117.904(7)
O–W–O	106.84(16)–111.44(15)

The coordination environments of the two crystallographically distinct Pb^{2+} cations is nearly equal and may be described as distorted singly capped square pyramid (Figure 5). With 2.30–2.88 Å the Pb–O distances expectably fluctuate around the sum of the effective ionic radii of 2.55 Å.[11]

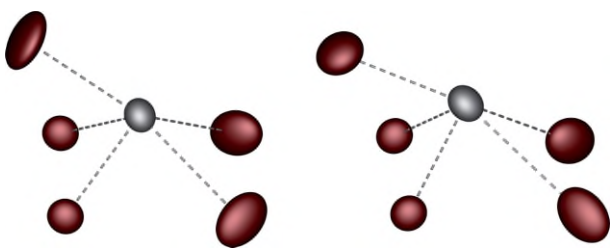

Figure 5. Coordination environment of Pb1 (left) and Pb2 (right) in $Pb_2O[WO_4]$; lead grey, oxygen red; all atoms are drawn with their displacement ellipsoids at a 95 % probability level.

Phase Transition Monitored by Raman Spectroscopy and PXRD

The phase transition in Pb_2WO_5 was already examined by *Fujita* et al.[8] which found a transition temperature of 330 ± 10 °C by DSC measurements. We monitored this conversion by temperature dependent Raman spectroscopy for the first time. Figure 6 visualizes the development of the symmetric W–O stretching vibration between 970–810 cm^{-1} in the temperature range 300–450 °C. As expected, the intensity of the $\nu_s(WO_6)$ band in $Pb_2[WO_5]$ at 845 cm^{-1} decreases with increasing temperature. But in the case of $Pb_2O[WO_4]$, a doublet arises, with maxima at 923 cm^{-1} and 902 cm^{-1}. Thereby the peak at 902 cm^{-1} is of higher intensity than the one at 923 cm^{-1} between 300 °C and the first measurement at 450 °C. After 10 min at 450 °C, the intensity ratio is inverted and after 90 min the peak at 902 cm^{-1} is nearly vanished. This suggests the presence of an intermediate state during the reconstructive phase transition from chains of corner-sharing WO_6 octahedra in $Pb_2[WO_5]$ to single WO_4 tetrahedra in $Pb_2O[WO_4]$.

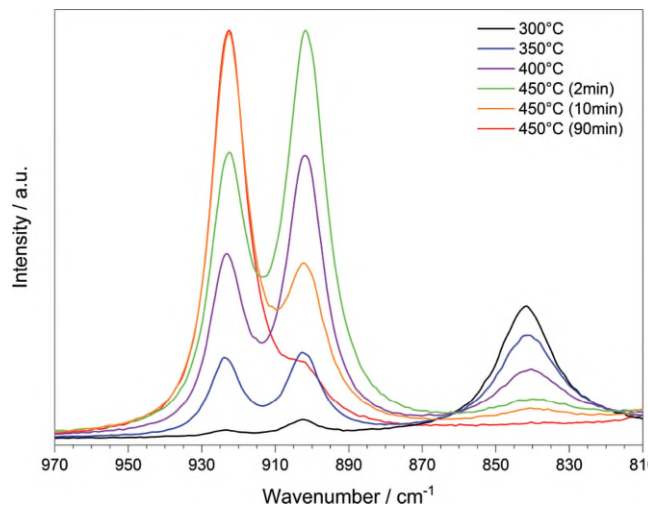

Figure 6. Temperature dependent Raman spectra of the phase transition from $Pb_2[WO_5]$ to $Pb_2O[WO_4]$ in the region 300–450 °C; only the W–O stretching vibrations are shown, the intensities are normalized.

Thus we also performed temperature dependent powder X-ray diffraction experiments (Figure 7), but we could not identify any further phase. In our experiment the transition

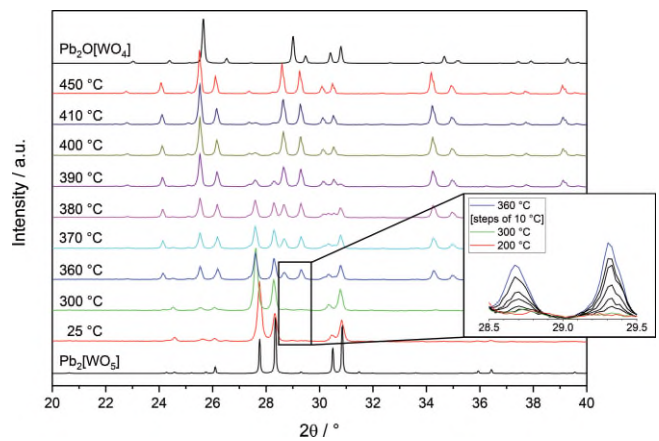

Figure 7. Temperature dependent powder XRD of the phase transition from $Pb_2[WO_5]$ to $Pb_2O[WO_4]$ in the region 25–500 °C; the inset emphasises the onset of the conversion between 200 and 360 °C.

starts roughly above 300 °C and is finished at approximately 450 °C.

The reconversion during cooling was observed either weakly or not at all, which matches with previous descriptions of this process. As described by *Fujita* et al. this is probably due to the strong dependence of the phase transition on the crystallite size of the sample, indicating a kinetic inhibition. Only large crystals of the high temperature modification easily complete the phase transition to the low temperature form and thereby crumble to a microcrystalline powder, while small crystallites of the high temperature form rather remain in this modification.

So it is rather easy to obtain a powder sample of $Pb_2O[WO_4]$ by heating several times to 400–600 °C with intermediate cooling to room temperature and grinding. Whereas to obtain a pure $Pb_2[WO_5]$ sample, one has to grow large crystals of the high temperature modification first, which convert ideally completely upon cooling. Thus it is interesting that we were able to obtain single crystals (large enough for single-crystal X-ray diffraction) by quenching the sample from 500 °C to room temperature. Already *Fujita* et al. had done quenching experiments and described a gradually change from $Pb_2O[WO_4]$ to $Pb_2[WO_5]$ at room temperature for quenched samples, which they monitored by powder X-ray diffraction. While they used sealed gold ampoules for their experiments, we put the open platinum crucible containing the powder directly into demin. water. Probably the thus increased cooling rate prevented the crumbling of the crystallites during or after the phase transformation by internal tensions.

A Crystallographic View on the Phase Transition

The unit cell of the low-temperature polymorph $Pb_2[WO_5]$ (LT) is related to the high-temperature one $Pb_2O[WO_4]$ (HT) via the transformation:

$-2\mathbf{c}_{HT}$, $\mathbf{b}_{HT}$, $\mathbf{a}_{HT} + 2\mathbf{c}_{HT}$

origin shift: (0; –¼; ½)

with a simultaneous shrinking by approx. 4 and 20 % of the obtained *a* and *c* axes, respectively. During the phase transition thus a quite strong stress is released causing the break-down of most of the crystals. Although there is a close geometric relationship between both crystal structures, no formal symmetry relationship between both is given and accordingly the phase transition cannot be described via a group-subgroup relationship. The transformation shows that the lead atoms not surprisingly almost do not change their positions, only a small shift is observed for O3 (HT) yielding O2 and O5 (LT), which are distorted tetrahedrally coordinated by a tungsten and three lead atoms. The remaining atoms show not surprisingly more or less large shifts, since the coordination number around the tungsten atoms increases from four to six (Tables S8, S9 and Figure S2, Supporting Information).

Electrostatic Calculations

We also checked the structure model of $Pb_2[WO_5]$ for electrostatic reasonability using calculations based on the MAPLE concept (MAPLE = Madelung Part of Lattice Energy).[12–14] A structure model is considered as electrostatically consistent if the sum of MAPLE values of chemically similar compounds deviates from the MAPLE value of the compound of interest by less than 1 %. According to our calculations the structure model thus shows electrostatic consistency (Table 3).

Table 3. Result of the MAPLE calculations for $Pb_2[WO_5]$ compared with the MAPLE calculations on PbO (ICSD no. 15403)[18] and WO_3 (ICSD no. 16080).[19]

MAPLE ($Pb_2[WO_5]$)		33269
MAPLE (PbO)	3636	
MAPLE (WO_3)	26087	
MAPLE (2 PbO + WO_3)		33359
Δ		0.27 %

DFT Calculations

The lattice parameters for the $Pb_2[WO_5]$ and $Pb_2O[WO_4]$ structures are overestimated by DFT-PBE and hybrid-HSE06 calculations (Table S3, Supporting Information). An insulating ground state is obtained for both high- and low-temperature polymorphs with both functionals. The calculated bandgaps (HSE06) coincide very well with the experimentally determined: 3.26 eV for $Pb_2[WO_5]$ and 3.87 eV for $Pb_2O[WO_4]$. The different bonding situation for the high- and low-temperature structure is revealed by the atomic site projected density of states (DOS) (see Figure 8 and Figure 9). In $Pb_2O[WO_4]$ the O1 atoms within the edge-sharing OPb_4 tetrahedral chains show a large overlap with the Pb atoms from –15 to –17 eV and slightly below the Fermi level, whereas O2, O3, and O4 exhibit higher DOS at –5 eV corresponding to bonding with W to form WO_4 tetrahedra. Octahedral coordination of W in $Pb_2[WO_5]$ features a broader DOS of the W-d-orbitals.

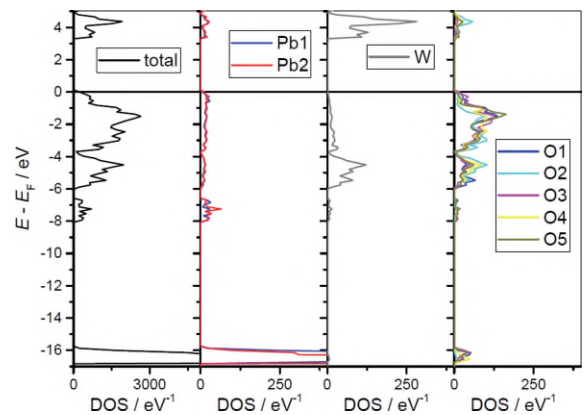

Figure 8. Atomic site projected density of states (DOS) of $Pb_2[WO_5]$.

Infrared and Raman Spectroscopy

The IR and Raman spectra of $Pb_2[WO_5]$ and $Pb_2O[WO_4]$ (Figure 10 and Figure 11) were recorded between 4000–

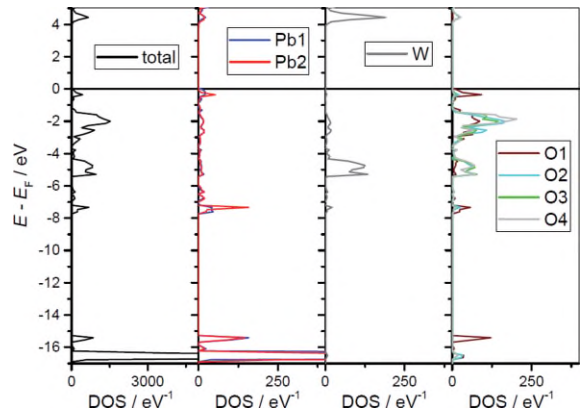

Figure 9. Atomic site projected density of states (DOS) of $Pb_2O[WO_4]$.

400 cm^{-1} (IR) and 1800–35 cm^{-1} (Raman) on powder samples. Above 1200 cm^{-1} no absorption bands were recorded. The spectra of $Pb_2[WO_5]$ (Figure 10) comprise symmetric stretching vibrations of the WO_6 octahedra in the region 900–750 cm^{-1} with the main band at 845 cm^{-1}. The asymmetric stretching vibrations lie in the range of 750–500 cm^{-1} followed below by several bending vibrations. In $Pb_2O[WO_4]$ (Figure 11) the stretching vibrations is at 923 cm^{-1}, whereas the asymmetric stretching vibrations are in the region 825–750 cm and the bending vibrations follow from 450–250 cm^{-1}. The strong Raman band at 145 cm^{-1} is due to the rotation of the complete WO_4 tetrahedron.

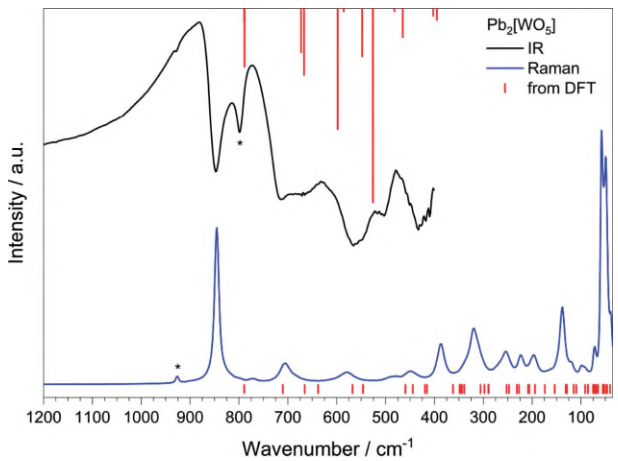

Figure 10. IR (black) and Raman (blue) spectra of $Pb_2[WO_5]$; the red bars represent the respective IR and Raman modes calculated by DFT; the peaks marked by an asterisk (*) belong to the side phase $Pb_2O[WO_4]$.

Temperature dependent Raman spectra pointing out the development of the symmetric W–O stretching vibrations during the phase transition from $Pb_2[WO_5]$ to $Pb_2O[WO_4]$ are shown in Figure 6. Beside the expected shift of the symmetric W–O stretching mode from WO_6 to WO_4, the spectra feature a third peak arising and vanishing during the phase transition suggesting the occurrence of an intermediate product.

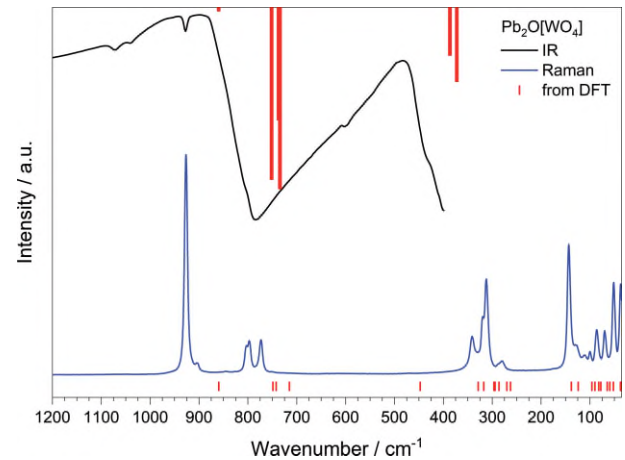

Figure 11. IR (black) and Raman (blue) spectra of $Pb_2O[WO_4]$; the red bars represent the respective IR and Raman modes calculated by DFT.

UV/Vis Spectroscopy

The UV/Vis reflectance spectrum of $Pb_2[WO_5]$ (Figure 12) comprises one absorption edge centred at 386 nm. The optical bandgap is determined as 3.4 eV [calcd. 3.3(1) eV]. The optical bandgap of $Pb_2O[WO_4]$ is determined as 3.9 eV [calcd. 3.8(1) eV]. According to our DFT calculations the band–band transition leading to the strong absorption bands can be classified as charge-transfer transition from occupied oxygen and Pb^{II} states into unoccupied tungsten states. Moreover, we would expect higher charge-transfer energy for the tetrahedrally coordinated tungsten species since the charge difference is smaller there reducing the urge to balance this difference at least temporarily.

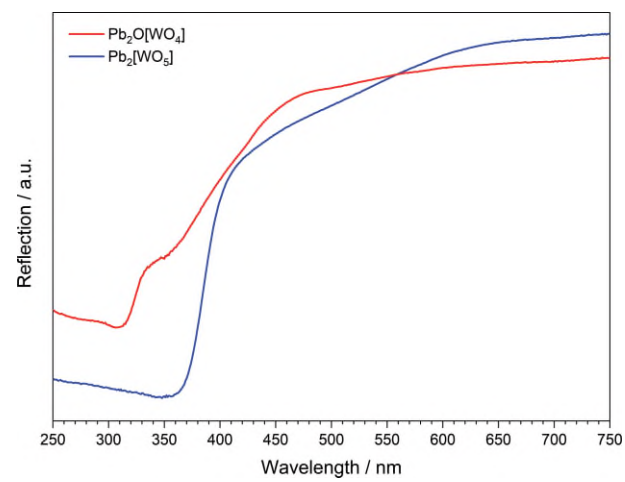

Figure 12. UV/Vis reflectance spectra of $Pb_2O[WO_4]$ (red) and $Pb_2[WO_5]$(blue).

Compared with the charge-transfer energies in the similar tungstates $M_2[WO_5]$ (M = Sr, Ba) these match very well with 4.0 and 3.9 eV to the data of $Pb_2[WO_5]$ comprising octahedral WO_6 moieties.

Conclusions

Pb_2WO_5 was found to exist in two modifications, a HT form, i.e. $Pb_2O[WO_4]$, and the LT-form $Pb_2[WO_5]$. We confirmed previous results but were able to follow the phase transition by temperature-dependent Raman spectroscopy assisted by temperature-dependent PXRD. Moreover, we could assign all relevant vibrational modes to observed frequencies. The phase-transition from HT to LT form proved to be inhibited kinetically making it very difficult to obtain single-crystals suited for the very first diffraction study on $Pb_2[WO_5]$ based on single-crystals; based on these data we could exclude similar strange effects on the thermal displacement parameters and clearly identify a new structure type.

Most interesting for us are the optical properties, since both forms should provide efficient charge-transfer energies suitable for absorbing UV radiation to be used for antenna phosphors in the near future. Our thoughts are confirmed by the spectroscopic results showing strong charge-transfer transitions from occupied oxygen and lead states into empty tungsten states. As primarily expected and confirmed by our results and calculations, these energies increase with tungsten's coordination number and is in line with our previous results in the similar tungstates $M_2[WO_5]$ (M = Sr, Ba).

Experimental Section

Synthesis of Single-Crystals: A single-crystal of $Pb_2[WO_5]$ was obtained by thoroughly grinding 2 M of PbO (≥ 99 %, Riedel-de Haën) with 1 M of WO_3 (99.9 %, Fluka) and heating the powder in a platinum crucible to 840 °C with a heating rate of 100 K·h^{-1}. The sample was held at this temperature for 2 d before it was cooled down to 500 °C with 50 K·h^{-1}. From this temperature the crucible was quenched manually to room temperature by putting the crucible from the furnace into a beaker with deionized water.

In the case of $Pb_2O[WO_4]$ a different lead source was used [$Pb(NO_3)_2$, 99.4 %, Merck] and a differing temperature program. The sample was heated to 800 °C with a heating rate of 100 K·h^{-1} and held at this temperature for 24 h. Afterwards the sample was cooled to 400 °C in 4 h, then to 270 °C in 13 h, where it was tempered another 12 h. In the end the sample was cooled to room temperature with 50 K·h^{-1}.

Synthesis of Powder Samples: A powder sample containing exclusively the low temperature form $Pb_2[WO_5]$ was obtained by a two-step synthesis. After thorough grinding, the mixture of 2.1 M of PbO and 1 M of WO_3 was distributed in a corundum crucible and loosely covered with a corundum plate as diffusion barrier. In a first step, the crucible was heated to 800 °C with 50 K·h^{-1} and kept at this temperature for 36 h until being slowly cooled to room temperature with 50 K·h^{-1}. In the second step, the newly ground product was heated to 910 °C and held for 1 h before cooling with 1 K·h^{-1} to 880 °C. From there it was cooled to room temperature again with 50 K·h^{-1}.

A pure sample of the high temperature modification $Pb_2O[WO_4]$ was obtained by heating a sample of the low temperature form several times to 600 °C with intermediate steps of cooling to room temperature and grinding.

Crystal Structure Determination: Crystals of both the low and high temperature modification were measured with a Bruker D8 Venture diffractometer equipped with a SMART APEXII 4k CCD detector, using Mo-K_α radiation; the data were corrected for absorption by applying a multi-scan approach. For the according solution of the crystal structures of both compounds direct methods were employed, using the SHELXTL program package[20] and refined with anisotropic displacement parameters for all atoms. $Pb_2O[WO_4]$ was refined as a 2-component twin. Details of the X-ray data collection are summarized in Table 4 for both compounds. Further crystal data such as atomic positions and displacement parameters are listed in the Supporting Information in Tables S4 and S5 for $Pb_2[WO_5]$ and in Tables S6 and S7 for $Pb_2O[WO_4]$.

Table 4. Crystal data and details of structure refinements of $Pb_2[WO_5]$ and $Pb_2O[WO_4]$.

	$Pb_2[WO_5]$	$Pb_2O[WO_4]$
Temperature /°C	24(2)	24(2)
M /g·mol^{-1}	678.23	678.23
Crystal system	monoclinic	monoclinic
Space group	$C2/c$ (no. 15)	$C2/m$ (no. 12)
a /Å	14.0996(4)	14.2126(4)
b /Å	5.8579(2)	5.80150(10)
c /Å	12.6877(4)	7.3477(2)
β /°	114.3569(13)	113.9402(7)
V /Å^3	954.66(5)	553.73(2)
Z	8	4
ρ(X-ray) /g·cm^{-3}	9.438	8.136
Crystal dimensions / mm^3	0.040 × 0.010 × 0.005	0.061 × 0.040 × 0.028
Color and shape	colorless needle	colorless block
μ /mm^{-1}	94.327	81.312
F(000)	2224	1112
Radiation (λ /Å)	Mo–K_α (0.71073)	Mo–K_α (0.71073)
Diffractometer	Bruker D8 Venture	Bruker D8 Venture
Abs. corr.	multi-scan	multi-scan
Min. / max. transmission	0.4830 / 0.7461	0.2943 / 0.7503
Index range	±18 / ±7 / ±16	–28 / 0 / 0–25 / 11 / 14
Theta range	3.172–27.498	3.033–44.998
No. coll. refl. / ind. data	14951 / 1094	5096 / 5096
Ratio of twin domains	–	77.3(1) : 22.7(1)
Parameter / restraints	74 / 0	47 / 0
Obs. refl. ($I > 2\sigma$) / R_{int}	1005 / 0.042	4424 / –
R (all data)	R_1 = 0.040, wR_2 = 0.068	R_1 = 0.035, wR_2 = 0.055
Weighting scheme	$w^{-1} = \sigma^2 F_o^2$ + (0.0082 P)^2 + 242.7911 P $P = (F_o^2 + 2F_c^2)/3$	$w^{-1} = \sigma^2 F_o^2$ + (0.0216 P)^2 + 3.8471 P; $P = (F_o^2 + 2F_c^2)/3$
GooF	1.166	1.051
Min. / max. res. density / e$^-$·Å^{-3}	–3.53 / 3.38	–2.43 / 3.44

Further details of the crystal structures investigations may be obtained from the Fachinformationszentrum Karlsruhe, 76344 Eggenstein-Leopoldshafen, Germany (Fax: +49-7247-808-666; E-Mail: crysdata@fiz-karlsruhe.de, http://www.fiz-karlsruhe.de/request for deposited data.html) on quoting the depository numbers CSD-433569 ($Pb_2[WO_5]$) and CSD-433570 ($Pb_2O[WO_4]$).

Powder X-ray Diffraction: Powder X-ray diffraction measurements were recorded with a PANalytical Empyrean diffractometer equipped with a PIXcel^{3D} 2 × 2 detector. This device was also used for temperature dependent measurement in Bragg-Brentano geometry with an

Anton Paar XRK 900 reaction chamber which allowed measurements in nitrogen atmosphere and a temperature range up to 900 °C.

The temperature profile of the temperature dependent XRD measurement (Figure 7) was: heat with 10 K·min^{-1} to the desired temperature and hold it, after a waiting time of 5 min a 20 min measurement started. Data were acquired at 25 °C, 100 °C, 200 °C, 300 °C and every 10 K between 310 °C and 450 °C. During cooling only at 300 °C, 200 °C, 100 °C and 25 °C pattern were recorded. During this, the sample of $Pb_2[WO_5]$ transformed to $Pb_2O[WO_4]$ and retained completely in this modification after cooling to room temperature.

The recorded patterns of both phases are compared to their respective calculated ones in Figures S3 and S4 (Supporting Information).

Density Functional Theory Calculations: Quantum chemical calculations were performed in the framework of density functional theory (DFT) using a linear combination of Gaussian-type functions (LCGTF) Scheme as implemented in CRYSTAL14.[21,22] The total energy calculations including full structural optimizations and subsequent calculations of the vibrational frequencies were performed with the GGA (PBE)[23] xc-functional. Furthermore, the electronic structures were tested by the calculations including full structural relaxations with the exact exchange functional HSE06[24,25] which includes a Hartree-Fock term in the exchange part. The convergence criterion considering the energy was set to 1×10^{-8} a.u. with a *k*-mesh sampling of $8 \times 8 \times 8$ for $Pb_2O[WO_4]$ and $6 \times 6 \times 6$ for $Pb_2[WO_5]$. Optimized effective core potential basis sets were applied for Pb and W,[26,27] the description of the oxygen atoms was carried out by an all-electron basis.[28] Vibrational frequencies calculations with IR intensities were run on fully optimized structural models so that no imaginary frequency was obtained. For the Raman spectrum, only the band positions were calculated. The modes were visualized and analyzed for all atoms. $Pb_2O[WO_4]$ was refined as a 2-component with the J-ICE application.[29]

The optimized cell parameters obtained by DFT calculations are listed in Table S3 (Supporting Information)

Spectroscopy: IR spectra were recorded with a Bruker EQUINOX 55 FT-IR-Spectrometer equipped with a Platinum ATR unit in range 4000–400 cm^{-1} with a resolution of 4 cm^{-1} and 32 scans. Raman spectra were recorded with a Thermo Scientific DXR Raman-Microscope in the range 1800–35 cm^{-1} using a 532 nm laser operated with 10 mW power (10–fold magnification, 50 µm pinhole aperture, high resolution grating (1800 lines mm^{-1}), spectral resolution 1 cm^{-1}). For temperature dependent measurements a Linkam DSC 600 Stage was used to heat the sample. UV/Vis spectra were recorded in reflection geometry with a Varian Cary 300 Scan UV/Vis spectrometer.

Supporting Information (see footnote on the first page of this article): figures illustrating structure relationships between HT and LT phase and the coordination environments of lead, tables containing details about the theoretical and MAPLE calculations, atomic coordinates and respective thermal displacement parameters and figures presenting powder diffraction patters.

Acknowledgements

F.P. thanks the Computer Service Group at MPI-FKF (Stuttgart, Germany) for providing computational resources.

Keywords: Tungstate; Lead; Phase transitions

References

[1] S. G. Jantz, F. Pielnhofer, M. Dialer, H. A. Höppe, *Z. Anorg. Allg. Chem.* **2017**, in press.
[2] M. Daub, K. Kazmierczak, H. A. Höppe, H. Hillebrecht, *Chem. Eur. J.* **2013**, *19*, 16954.
[3] P. Gross, A. Kirchhain, H. A. Höppe, *Angew. Chem. Int. Ed.* **2016**, *55*, 4353.
[4] M. Daub, A. J. Lehner, H. A. Höppe, *Dalton Trans.* **2012**, *41*, 12121.
[5] Inorganic Crystal Structure Database, Version 2017–1, Fachinformationszentrum Karlsruhe, **2017**.
[6] F. Bosselet, B. Mentzen, J. Bouix, *Mater. Res. Bull.* **1985**, *20*, 1329.
[7] R. DeVries, J. Fleischer, *Mater. Res. Bull.* **1970**, *5*, 87.
[8] T. Fujita, K. Muramatsu, *Mater. Res. Bull.* **1979**, *14*, 5.
[9] S. Miyazawa, H. Iwasaki, *J. Cryst. Growth* **1971**, *8*, 359.
[10] M. Kunz, I. D. Brown, *J. Solid State Chem.* **1995**, *115*, 395.
[11] R. D. Shannon, *Acta Crystallogr., Sect. B* **1976**, *32*, 751.
[12] R. Hoppe, *Angew. Chem. Int. Ed. Engl.* **1966**, *5*, 95.
[13] R. Hoppe, *Angew. Chem. Int. Ed. Engl.* **1970**, *9*, 25.
[14] R. Hübenthal, *MAPLE*, Program for the Calculation of the Madelung Part of Lattice Energy, Gießen, Germany, **1993**.
[15] K. Sahl, *Z. Kristallogr.* **1970**, *132*, 99.
[16] T. Balić-Žunić, E. Makovicky, *Acta Crystallogr., Sect. B* **1996**, *52*, 78.
[17] E. Makovicky, T. Balić-Žunić, *Acta Crystallogr., Sect. B* **1998**, *54*, 766.
[18] M. Kay, *Acta Crystallogr.* **1961**, *14*, 80.
[19] B. O. Loopstra, H. M. Rietveld, *Acta Crystallogr., Sect. B* **1969**, *25*, 1420.
[20] G. Sheldrick, *Acta Crystallogr., Sect. A* **2008**, *64*, 112.
[21] R. Dovesi, V. R. Saunders, C. Roetti, R. Orlando, C. M. Zicovich-Wilson, F. Pascale, B. Civalleri, K. Doll, N. M. Harrison, I. J. Bush, P. D'Arco, M. Llunell, M. Causà and Y. Noël, *CRYSTAL14* User's Manual, University of Torino, Torino, Italy, **2014**.
[22] R. Dovesi, R. Orlando, A. Erba, C. M. Zicovich-Wilson, B. Civalleri, S. Casassa, L. Maschio, M. Ferrabone, M. D. L. Pierre, P. D'Arco, Y. Noël, M. Causà, M. Rérat, B. Kirtman, *Int. J. Quantum Chem.* **2014**, *114*, 1287.
[23] J. P. Perdew, K. Burke, M. Ernzerhof, *Phys. Rev. Lett.* **1996**, *77*, 3865.
[24] A. D. Becke, *Phys. Rev. A* **1988**, *38*, 3098.
[25] J. Heyd, G. E. Scuseria, M. Ernzerhof, *J. Chem. Phys.* **2003**, *118*, 8207.
[26] G. Sophia, P. Baranek, C. Sarrazin, M. Rérat, R. Dovesi, *Phase Transitions* **2013**, *86*, 1069.
[27] Basis set ECP60MHF for W, ECP60MHF, http://www.tc.uni-koeln.de/PP/clickpse.en.html.
[28] J. Scaranto, S. Giorgianni, *J. Mol. Struct.* **2008**, *858*, 72.
[29] P. Canepa, R. M. Hanson, P. Ugliengo, M. Alfredsson, *J. Appl. Crystallogr.* **2014**, *47*, 225.